Manuscript No. MRMP-D-16-00113R1, 1st revision

Feasibility of *in vivo* three-dimensional T_2^* mapping using dicarboxy-PROXYL and CW-EPR-based single-point imaging

Harue Kubota[1] • Denis A. Komarov[1] • Hironobu Yasui[2] • Shingo Matsumoto[1] •

Osamu Inanami[3] • Igor A. Kirilyuk[4] • Valery V. Khramtsov[5] • Hiroshi Hirata[1*]

1. Division of Bioengineering and Bioinformatics, Graduate School of Information Science and Technology, Hokkaido University, North 14, West 9, Kita-ku, Sapporo, 060-0814, Japan

2. Central Institute of Isotope Science, Hokkaido University, North 15, West 7, Kita-ku, Sapporo, 060-0815, Japan

3. Laboratory of Radiation Biology, Graduate School of Veterinary Medicine, Hokkaido University, North 18, West 9, Kita-ku, Sapporo, 060-0818, Japan

4. N. N. Vorozhtsov Novosibirsk Institute of Organic Chemistry, 9, Ac. Lavrentieva Ave., Novosibirsk, 630090, Russia

5. Department of Biochemistry, West Virginia University, Robert C. Byrd Health Sciences Center, 1 Medical Center Drive, Morgantown, West Virginia 26506, USA

* Corresponding author:
Hiroshi Hirata, Ph.D.
Phone: +81-11-706-6762
E-mail: hhirata@ist.hokudai.ac.jp

Abstract

Objectives The aim of this study was to demonstrate the feasibility of *in vivo* three-dimensional (3D) relaxation time T_2^* mapping of a dicarboxy-PROXYL radical using continuous-wave electron paramagnetic resonance (CW-EPR) imaging.

Materials and Methods Isotopically substituted dicarboxy-PROXYL radicals, 3,4-dicarboxy-2,2,5,5-tetra($^2H_3$)methylpyrrolidin-(3,4-$^2H_2$)-(1-^{15}N)-1-oxyl (^{2}H,^{15}N-DCP) and 3,4-dicarboxy-2,2,5,5-tetra($^2H_3$)methylpyrrolidin-(3,4-$^2H_2$)-1-oxyl (^{2}H-DCP), were used in this study. A clonogenic cell survival assay was performed with ^{2}H-DCP radical using squamous cell carcinoma (SCC VII) cells. The time-course of EPR signal intensities of intravenously injected ^{2}H,^{15}N-DCP and ^{2}H-DCP radicals were determined in tumor-bearing hind legs of mice (C3H/HeJ, male, *n*=5). CW-EPR-based single-point imaging (SPI) was performed for 3D T_2^* mapping.

Results ^{2}H-DCP radical did not exhibit cytotoxicity at concentrations below 10 mM. The *in vivo* half-life of ^{2}H,^{15}N-DCP in tumor tissues was 24.7 ± 2.9 min (mean ± standard deviation (SD), *n*=5). *In vivo* time-course of the EPR signal intensity of ^{2}H,^{15}N-DCP radical showed a plateau of 10.2 ± 1.2 min (mean ± SD), where the EPR signal intensity remained at more than 90% of the maximum intensity. During the plateau, *in vivo* 3D T_2^* maps with ^{2}H,^{15}N-DCP were obtained from tumor-bearing hind legs with a total acquisition time of 7.5 min.

Conclusion EPR signals of ^{2}H,^{15}N-DCP persisted long enough after bolus intravenous injection to conduct *in vivo* 3D T_2^* mapping with CW-EPR-based SPI.

Keywords: nitroxyl radical • clonogenic assay • *in vivo* nitroxyl radical kinetics • *in vivo* EPR • T_2^* mapping • single-point imaging

Introduction

Non-invasive visualization of the oxygen content in biological tissues is important for understanding both physiological and pathophysiological conditions [1]. In particular, under conditions of low oxygenation, called hypoxia, tumor tissues are known to be resistant to radiation therapy [2,3]. Therefore, there is significant interest in the development of new technologies for determining the oxygen partial pressure, pO_2 [4–6]. Electron paramagnetic resonance (EPR) spectroscopy is a non-invasive method for the quantitative determination of pO_2 [7–10]. EPR-based oxygen mapping requires a soluble spin probe that is sensitive to molecular oxygen. Two major groups of oxygen-sensitive spin probes have been used for EPR oxygen mapping: nitroxyl radicals have been used for pO_2 measurements since the 1970's [11–15], and trityl radicals were introduced for EPR oxygen mapping in 1998 [16–18].

The oxygen partial pressure, pO_2, can be mapped by monitoring the change in the relaxation time or EPR line-width of an unpaired electron in the spin probe. The relaxation time is affected by the unpaired electrons in molecular oxygen [19]. Various approaches to mapping of the relaxation time or line-width of the spin probe use either spectral-spatial imaging or single-point (constant-time) imaging (SPI) in continuous-wave (CW) EPR [20,21], and either SPI or inversion recovery with electron spin echo readout in pulsed EPR [22,23]. For pulsed EPR imaging, a spin probe with a long relaxation time (> 1 μs) is essential. For this reason, trityl radicals are most commonly used for pO_2 mapping by pulsed EPR techniques [24,25]. The only report of pO_2 mapping using nitroxyl radical (^{15}N-substituted perdeuterated TEMPONE) and 300-MHz pulsed EPR was provided by Hyodo *et al*. [26]. In contrast, CW-EPR can use nitroxyl radicals with shorter relaxation times (< 0.5 μs). From a technical perspective regarding pO_2 mapping, while four-dimensional (4D) CW-EPR imaging (three dimensions in the spatial domain and one dimension in the spectral domain) takes a longer time than pulsed EPR imaging, it has been shown to be feasible for use in *in vivo*

animal experiments [27]. The comparatively long data-acquisition time remains one of the major drawbacks of 4D CW-EPR imaging. The acquisition time is important in *in vivo* animal experiments because of elimination of the applied spin probe and the corresponding decay of the EPR signal in the subject animals. Thus, the feasibility of 4D CW-EPR imaging for the mapping of tumor oxygenation using nitroxyl radicals primarily depends on the life-time of the spin probe in the subject animals and the time required for image acquisition.

The use of CW-EPR for 4D spectral-spatial imaging was first reported by Kuppusamy *et al*. in 1995 [28]. In that study, isolated rat hearts were visualized with 4D EPR imaging using glucose char. The total image-acquisition time for 1000 projections was 104 minutes. Elas *et al*. [27] performed 4D CW-EPR imaging in animal tumors using a trityl radical (OX031). The acquisition time for 512 projections was approximately 20 minutes, with an average of two sweeps per projection. 2D line-width maps of tumor-bearing mouse legs were obtained by CW-EPR-based SPI using a trityl radical (OX063) with a total of 256 projections and 2-s field scanning (the acquisition time was more than 8 minutes) [21]. Based on these previous results, the speed of CW-EPR imaging needs to be further accelerated for use in animal experiments. Four-dimensional CW-EPR imaging should be easy to apply to *in vivo* pO_2 mapping in animal tumors, if it could be performed within the time-window determined by the intensity of EPR signal after a bolus injection of nitroxyl radical into a subject animal.

Isotopically substituted dicarboxy-PROXYL has recently been introduced for use in EPR oxygen mapping [29]. While the oxygen sensitivity of this radical and its use in EPR oxygen mapping in isolated rat hearts have been reported, its toxicity and *in vivo* time-course of the EPR signal intensity remain unclear. The EPR signal intensity decay of *cis*-dicarboxy-PROXYL radical has been reported for a tumor-bearing mouse model [30]. While the *cis*- and *trans*-isomers of dicarboxy-PROXYL radical have been examined with regard to their solubility [30], a racemic mixture of isotopically substituted

trans-dicarboxy-PROXYL was not investigated with respect to toxicity or *in vivo* clearance. Moreover, different tumor models and tumor size may also influence the time-course of EPR signal intensity of injected radicals.

The purpose of this work was to examine the feasibility of *in vivo* 4D CW-EPR imaging using the dicarboxy-PROXYL. In this article, we report the results of a clonogenic cell survival assay and the *in vivo* time-course of EPR signal intensity of isotopically substituted dicarboxyl-PROXYL radicals. In addition, we show that *in vivo* 4D EPR imaging in mice is feasible with the isotopically substituted dicarboxyl-PROXYL radical and CW-EPR-based SPI. 3D maps of the relaxation time T_2^* in living mice were obtained within 7.5 minutes using CW-EPR-based SPI after a bolus injection of the isotopically substituted dicarboxyl-PROXYL radical.

Since the SPI modality has fewer artifacts than back-projection reconstruction, CW-EPR-based SPI was used in this work. CW-EPR-based SPI visualizes T_2^* instead of true T_2. Most previous studies on SPI-based pO_2 mapping have been conducted with T_2^*mapping, and only a few studies of pO_2 mapping with the SPI modality have been based on T_2 [31]. While T_2^*-based EPR oxygen mapping requires the proper calibration of T_2^* to pO_2 for a given resonator, gradient settings, and decay time-window, T_2^* is inversely proportional to the apparent EPR line-width and to pO_2 [22].

Materials and Methods

Spin probe

The nitroxyl radicals *trans*-3,4-dicarboxy-2,2,5,5-tetra($^2H_3$)methylpyrrolidin-(3,4-$^2H_2$)-(1-^{15}N)-1-oxyl (^2H,^{15}N-DCP) and *trans*-3,4-dicarboxy-2,2,5,5-tetra($^2H_3$)methylpyrrolidin-(3,4-$^2H_2$)-1-oxyl (^2H-DCP) were used as spin probes. Their chemical structures are shown in Fig. 1(a). The

radicals were synthesized as described in the literature [29]. Racemic mixtures of the two enantiomeric forms of the radicals were used for this study. First-derivative EPR absorption spectra of the radicals are given in Figs. 1(b) and 1(c).

Clonogenic assay

A clonogenic cell survival assay was performed with four different concentrations of ^{2}H-DCP radical using squamous cell carcinoma (SCC VII) cells [32]. The assay was performed with only one isotopic form of the radical, since we expected that ^{2}H,^{15}N-DCP would have the same cytotoxicity as ^{2}H-DCP. Solutions of ^{2}H-DCP with concentrations of 0, 0.1, 1.0, 10 and 100 mM in phosphate-buffered saline were prepared and the pH was adjusted to 7.4 by the addition of NaOH. Petri dishes with 100 SCC VII cells were exposed to 2.5 mL of the ^{2}H-DCP solutions for 2 h in a CO_2 incubator at 37ºC. The cells were then washed and incubated for an additional week. Cell colonies were fixed with methanol and stained with Giemsa solution (Wako Pure Chemical Co., Tokyo, Japan). The next day, the number of colonies in the dish was counted and the fraction of surviving SCC VII cells was calculated. Three dishes were used for each concentration of ^{2}H-DCP radical.

Animal preparation

Six- to seven-week-old C3H/HeJ male mice (20–22 g) were purchased from Japan SLC (Hamamatsu, Japan). Murine SCC VII cells, derived from C3H mice [33], were maintained in α-minimum essential medium (Gibco-BRL/Invitrogen, Carlsbad, CA) supplemented with 10% fetal bovine serum (Filtron, Brooklyn, Australia) at 37ºC in 5% CO_2 /95% air. Approximately one million SCC VII cells were subcutaneously injected into the right hind leg. EPR experiments were performed 8 or 9 days after the implantation of SCC VII cells. Tumor volume (V) was estimated using linear calipers and the relationship V = (Length × Width ×

Depth) $\pi/6$. All experiments were performed in accordance with the 'Law for The Care and Welfare of Animals in Japan' and approved by the Animal Experiment Committee of Hokkaido University.

CW-EPR imager/spectrometer

A laboratory-built CW-EPR imager/spectrometer operating at 750 MHz was used for the spectroscopic measurements and imaging. The details of this EPR instrument have been reported previously [34,35]. Here we provide only a brief outline. The magnet system consists of a main permanent magnet (27 mT), a pair of field scanning coils and three pairs of field gradient coils for the X-, Y- and Z-directions. The field scanning and gradient coils were driven by computer-controlled bipolar power supplies. A multi-coil parallel-gap resonator (22 mm in diameter and 30 mm in length) and a reflection-type RF bridge were used for EPR detection [34,36]. EPR data acquisition and imaging were controlled using a laboratory-developed LabVIEW-based program (LabVIEW 8.5, National Instruments Corp., Austin, TX) on MacOS 10.5 and an Apple MacPro computer.

***In vivo* time-course of EPR signal intensity**

The EPR signal intensities of ^{2}H,^{15}N-DCP and ^{2}H-DCP radicals were examined using tumor-bearing mice (sample size n=5). Due to the different multiplicities of ^{2}H-DCP and ^{2}H,^{15}N-DCP, the time-course of EPR signal intensities of the radicals were examined by tracking the EPR signal intensities for both radicals simultaneously. A mixture of 50 mM ^{2}H,^{15}N-DCP and 50 mM ^{2}H-DCP in PBS was prepared for the measurements. The solution pH was adjusted to 7.4 by the addition of NaOH. Mice were anesthetized by the inhalation of 2–3% isoflurane and the tail vein was cannulated. Under the inhalation of isoflurane at 1–2%, a subject mouse was placed in the prone position on an animal holder. The tumor-bearing leg

of the mouse was inserted into the resonator of the CW-EPR spectrometer. Thirty seconds after the beginning of EPR signal acquisition, a mixture of the radicals (0.2 mmol/kg body weight for each probe) was intravenously injected via a tail vein as a bolus over 10 seconds. EPR spectra were collected over 60 minutes. The measurement parameters of EPR spectroscopy were as follows: duration of field scanning 0.5 s, magnetic field scanning 6 mT, amplitude of magnetic field modulation 0.1 mT, time constant of a lock-in amplifier 0.3 ms, incident RF power 5 mW, and number of data acquisition points 512 per scan.

***In vivo* EPR imaging**

Tumor-bearing legs of mice were measured with the 750-MHz CW-EPR imager. The mouse body temperature and respiration rate were monitored using a small animal monitoring and gating system (model 1030, SA Instruments, Inc., Stony Brook, NY), and body temperature was maintained at 37ºC with feedback-regulated heated airflow. Other conditions of animal handling were the same as for the measurements of probe clearance. ^{2}H,^{15}N-DCP (0.4 mmol/kg body weight) was intravenously injected as a bolus into a subject mouse. This dose level was chosen based on the results of preliminary experiments which showed that it gave *in vivo* 3D images with minimal noise. EPR acquisition was started 5 minutes thereafter. The central magnetic field was set to the peak at a lower field of two EPR absorption peaks of ^{2}H,^{15}N-DCP. The following measurement settings were used for EPR image acquisition: scan time 0.1 s, magnetic field scanning 2 mT, magnetic field modulation 30 μT, modulation frequency 90 kHz, time-constant of a lock-in amplifier 0.1 μs, number of data acquisition points 512 per scan, and incident RF power 5.5 mW. Incrementally ramped field gradients in equal steps were used for EPR image acquisition. The projections were acquired at 15 × 15 × 15 field gradients for the X-, Y- and Z-directions (total of 3375 projections). The maximum field gradient for each direction was 20 mT/m. The total acquisition time was 7.5 min.

Image reconstruction

Three-dimensional spatial images of EPR signals were reconstructed by inverse Fourier transform of 3D *k*-space data. The computation code was implemented according to reports on the SPI method by Subramanian *et al*. [22] and Matsumoto *et al.* [21]. EPR projections were integrated to obtain the absorption profile and the inverse Fourier transform was performed to calculate the free-induction decay signals. A series of time-dependent 3D spatial images were obtained by shifting the time-delay in the free-induction decay signals. Relaxation time T_2^* was calculated voxel by voxel by fitting the signal decay through the series of spatial images with an exponential function. When we computed the relaxation times, we used the *k*-space extrapolation method reported by Jang *et al*. [37] to keep the field-of-view (FOV) of the reconstructed images constant. The computation code was written in a Fortran 95 development environment (Absoft Pro Fortran 2016, Absoft Corp., Keego Harbor, MI) and run on an Apple MacPro computer.

Results

Cytotoxicity

The clonogenic assay was conducted to clarify the cytotoxicity of the DCP radicals. Figure 2 shows the results of the clonogenic assay of SCC VII cells with ^{2}H-DCP. The closed plots and error bars represent the means and standard deviations (SD) of the survival fraction (n=3). The survival fraction remained approximately 100% at radical concentrations below 10 mM and decreased to approximately 60% at a concentration of 100 mM.

***In vivo* time-course of EPR signal intensity**

To understand the elimination rates of the DCP radicals *in vivo*, the time-course of EPR

signal intensities was measured for tumor-bearing mice after a bolus intravenous injection of a mixture of $^{2}H,^{15}N$-DCP and ^{2}H-DCP. The experiments were performed when the tumor volumes were 933 ± 115 mm^3 (mean ± SD, *n*=5). Figure 3 shows a typical time-course of EPR signal intensities of $^{2}H,^{15}N$-DCP and ^{2}H-DCP measured in the tumor-bearing leg of a subject mouse. The EPR signals of the radicals appeared immediately after the intravenous injection, reached a maximum intensity at approximately 8 minutes and then gradually decayed (Fig. 3). The amount of time that the observed EPR signals had an intensity of more than 90% of their maximum was 10.2 ± 1.2 min for $^{2}H,^{15}N$-DCP and 10.7 ± 1.8 min for ^{2}H-DCP (mean ± SD). The maximum signal intensity of $^{2}H,^{15}N$-DCP was 1.7-fold higher than that of ^{2}H-DCP. The *in vivo* half-lives of the DCP probes were calculated by fitting the decay of EPR signal intensity with a monoexponential function. The calculated half-lives for $^{2}H,^{15}N$-DCP and ^{2}H-DCP were 24.8 ± 2.9 min and 24.5 ± 2.9 min (mean ± SD), respectively.

***In vivo* EPR imaging**

The feasibility of *in vivo* CW-EPR imaging (T_2^* mapping) based on SPI using the $^{2}H,^{15}N$-DCP radical as a spin probe was examined in several tumor-bearing mice with the 750-MHz CW-EPR imager. Figure 4(a) shows a photograph of the tumor-bearing right hind leg of a subject mouse. A 3D surface-rendered image of EPR signal intensities is shown in Fig. 4(b). The shape of the 3D image properly corresponds to the tumor-bearing right hind leg in the photograph in Fig. 4(a). Part of the tail was also visualized in Fig. 4(b). Figure 4(c) shows slice-selective EPR signal intensity maps that were generated from the 3D image in Fig. 4(b). The relaxation time T_2^* was calculated for the image data with a threshold of 40% of the maximum signal intensity. The T_2^* maps in Fig. 4(d) correspond to the intensity maps in Fig. 4(c). The results show that CW-EPR-based SPI can be used to visualize the three-dimensional spatial distribution and T_2^* maps of $^{2}H,^{15}N$-DCP radical in tumor-bearing mice. In the central

region of tumor tissues, a weak EPR signal was observed, as shown in Fig. 4(c) (panels for the XZ-plane and the XY-plane). This could be related to low blood flow and the low penetration of $^{2}H,^{15}N$-DCP radical into this region. This results in the absence of a T_2^* calculation in Fig. 4(d) (clearly seen in the panel for the XZ-plane), since the EPR signal intensity was below the threshold for T_2^* calculation.

Discussion

The concentration of $^{2}H,^{15}N$-DCP used for the EPR imaging experiments was 0.4 mmol/kg of mouse body weight. By taking into account the blood volume, we estimated that the average concentration of the radical in blood was below 5 mM. This value is considerably less than the concentration at which the survival fraction in the clonogenic assay decreases, as shown in Fig. 2. The fact that this concentration is far below the cytotoxicity level and the lack of mortality of the subject mice suggest that $^{2}H,^{15}N$-DCP and ^{2}H-DCP radicals did not have any toxic effect on the animals during the EPR experiments. However, a comprehensive analysis of the toxicology profiles of $^{2}H,^{15}N$-DCP and ^{2}H-DCP radicals would be important for future animal studies and potential clinical applications.

The EPR signal intensity for $^{2}H,^{15}N$-DCP radical showed a plateau of more than 90% of its maximum value that lasted for 10 to 11 minutes. This is long enough for data acquisition by CW-EPR-based SPI, which takes 7.5 minutes for $(15)^3$ projections. Dicarboxy-PROXYL radical was chosen based on its longer lifetime in animals due to its pyrrolidine ring structure and lower cell membrane permeability. Also, by using the dicarboxy-PROXYL and its ^{15}N-derivative, we could confirm that stable isotopic nitrogen-labeling in dicarboxy-PROXYL does not affect the time-course of the EPR signal intensity in animals, as one would expect. Our aim in investigating the time-course of EPR signal intensity was to identify an appropriate time-window for EPR image-acquisition in tumor tissues. While the Tofts model

can be used to estimate the overall time-course of an exogenously infused extracellular contrast agent such as gadolinium-diethylenetriamine penta-acetic acid (Gd-DTPA) [38], it is not necessarily needed for our purposes. As shown in Fig. 3, ^{15}N-substituted radical had a 1.7-fold higher peak-to-peak EPR signal intensity. Thus, the use of ^{2}H,^{15}N-DCP may be beneficial for *in vivo* EPR imaging, since it offers a significant improvement in the signal-to-noise ratio. Additionally, ^{2}H,^{15}N-DCP has a narrower absorption line-width than that of ^{2}H-DCP, and thus provides a better sensitivity to low oxygen concentrations.

The feasibility of *in vivo* 4D EPR imaging strongly depends on the toxicity and the rate of spin probe clearance, as well as on the time required for EPR data acquisition. The application of fast field scanning [34,35] in this work enabled 4D CW-EPR imaging with a total of 3375 projections and a data-acquisition time of 7.5 minutes. *In vivo* 3D T_2^* mapping using CW-EPR-based SPI was performed after a bolus injection of ^{2}H,^{15}N-DCP radical, as shown in Fig. 4.

^{2}H,^{15}N-DCP has characteristics that make it suitable for *in vivo* 3D T_2^* mapping. The synthesis of dicarboxy-PROXYL radical (hereafter abbreviated as DCP) was reported in 1982 [39], and it was later suggested as a potential contrast agent for nuclear magnetic resonance imaging [40]. DCP radical was also considered for use in neuroscience applications and EPR imaging of the mouse head [41]. Those authors suggested use of the ester derivative of DCP, *trans*-3,4-di(acetoxymethoxycarbonyl)-2,2,5,5-tetramethyl-1-pyrrolidinyloxyl, which can be converted to DCP intracellularly upon esterase hydrolysis. The chemical synthesis of ^{2}H,^{15}N-substituted carboxy-PROXYL radical has also been reported [42]. This radical was proposed for use in *in vivo* EPR imaging of the oxygen concentration. Isotopic substitution of the nitrogen atom of a nitroxyl fragment with ^{15}N and complete isotopic substitution of the protons with ^{2}H substantially increases the EPR signal intensity and significantly improves the oxygen sensitivity. More recently, the time-course of EPR signal intensity of *cis*-DCP was

reported for the tumor-bearing leg of a mouse [30]. In that study , FSa methylcholanthrine-induced fibrosarcoma cells were used as the tumor model. The average *in vivo* half-life of the EPR signal intensity of *cis*-DCP radical after intravenous injection was 21.4 ± 2.0 min. This value is slightly shorter than that in our study, and this difference may be due to the use of different radical isomers and different tumor models in the experiments. Redler *et al*. [30] also discussed the localization of DCP in tumor tissues. At physiological pH, DCP radical is present in the form of a dianion, and thus is expected to be mainly confined in the extracellular fluid. This can explain the comparatively long half-life of the EPR signal intensity of DCP radical *in vivo*.

Due to the recent progress in the acquisition speed of CW-EPR imaging [34,35] and the development of $^{2}H,^{15}N$-DCP radical [29], 3D CW-EPR-based T_2^* mapping has become available for use in living mice with a bolus injection of the radical. *In vivo* 3D T_2^* mapping is an important step toward pO_2 mapping using CW-EPR-based SPI. In this article, T_2^* maps were not converted to pO_2 maps, since the observed T_2^* values include the effects of pO_2 and the concentration of $^{2}H,^{15}N$-DCP. Studies on the quantitative detection of pO_2 through the use of CW-EPR-based SPI and isotopically substituted DCP radicals are now underway.

The variance of T_2^* for a uniform solution sample should be as small as possible to obtain T_2^* maps with greater precision. For example, 3D T_2^* maps for air-saturated and nitrogen gas-bubbled 3 mM $^{2}H,^{15}N$-DCP solutions (3 mL of PBS) gave values of 147 ± 2 ns and 192 ± 4 ns (mean ± SD) (data not shown), respectively, with our EPR imaging scanner and image-reconstruction procedure. Based on these T_2^* values, the difference between the mean values of T_2^* (45 ns) corresponds to 159 mmHg (pO_2 in air). If the SD of a T_2^* map for a uniform sample is 3 ns, a pO_2 map has a SD of approximately 10 mmHg. T_2^* is also related to the probe concentration. To determine the quantitative oxygen partial pressure pO_2 from T_2^* images, it is necessary to know the local concentration of the spin probe, $^{2}H,^{15}N$-DCP in

this case. The concentration-induced changes in T_2^* differ for the ^{15}N- and ^{14}N-labeled isotopic forms of the DCP radical. In the present study, we have demonstrated that the time-courses of the *in vivo* EPR signal intensity for the two radicals are identical, as would be expected from theory. If we assume a constant ratio of two isotopic forms in a subject animal, we believe that the application of a mixture of the DCP radicals to a subject animal would enable simultaneous measurements of the probe concentration and pO_2.

Conclusion

The present results demonstrated the feasibility of *in vivo* 3D T_2^* mapping by CW-EPR-based SPI with the application of $^{2}H,^{15}N$-DCP radical as a spin probe. The probe showed no significant cytotoxicity at concentrations below 10 mM. The *in vivo* half-life of the EPR signal intensity of $^{2}H,^{15}N$-DCP was approximately 25 minutes. The EPR signal of $^{2}H,^{15}N$-DCP persisted long enough for *in vivo* 4D EPR imaging after a single bolus injection of the probe.

Acknowledgements

This work was supported by JSPS KAKENHI Grant Number 26249057 (to HH).

Conflict of interest

The authors declare that they have no conflict of interest.

Authors' contributions

Kubota: Data collection, Data analysis

Komarov: Data collection, Data analysis

Yasui: Data collection, Data analysis

Matsumoto: Data collection, Data analysis

Inanami: Data collection

Kirilyuk: Data collection

Khramtsov: Protocol/project development

Hirata: Protocol/project development, Data management

References

1. Carreau A, Hafny-Rahbi BE, Matejuk A, Grillon C, Kieda C (2011) Why is the partial oxygen pressure of human tissues a critical parameter? Small molecules and hypoxia. J Cell Mol Med 15:1239–1253
2. Horsman MR (1998) Measurement of tumor oxygenation. Int J Radiat Oncol Biol Phys 42:701–704
3. Höckel M, Schlenger K, Aral B, Mitze M, Schäffer U, Vaupel P (1996) Association between tumor hypoxia and malignant progress in advanced cancer of the uterine cervix. Cancer Res 56:4509–4515
4. Clark LC Jr, Wolf R, Granger D, Taylor Z (1953) Continuous recording of blood oxygen tensions by polarography. J Appl Physiol 6:189–193
5. Peterson JI, Fitzgerald R, Buckhold DK (1984) Fiber-optic probe for in vivo measurement of oxygen partial pressure. Anal Chem 56:62–67
6. Mason RP, Rodbumrung W, Anticj PP (1996) Hexafluorobenzene: a sensitive ^{19}F NMR indicator of tumor oxygenation. NMR Biomed 9:125–134
7. Liu KJ, Gast P, Moussavi M, Norby SW, Vahidi N, Walczak T, Wu M, Swartz HM (1993) Lithium phthalocyanine: A probe for electron paramagnetic resonance oximetry in viable biological systems. Proc Natl Acad Sci USA 90:5438–5442
8. Halpern HJ, Yu C, Peric M, Barth E, Grdina DJ, Teicher BA (1994) Oxymetry deep in tissues with low-frequency electron paramagnetic resonance. Proc Natl Acad Sci USA 91:13047–13051
9. Zweier JL, Kuppusamy P (1988) Electron paramagnetic resonance measurements of free radicals in the intact beating heart: a technique for detection and characterization of free radicals in whole biological tissues. Proc Natl Acad Sci USA 85:5703–5707
10. Pandian RP, Parinandi NL, Ilangovan G, Zweier JL, Kuppusamy P (2003) Novel

particulate spin probe for targeted determination of oxygen in cells and tissues. Free Radic Biol Med 35:1138–1148

11. Hoff J, Deen R (1971) The influence of oxygen on the E.R.S. spectrum of a radiosensitizing nitroxide, Int J Radiat Biol 19: 499–501
12. Backer JM, Budker VG, Eremenko SI, Molin YN (1977) Detection of the kinetics of biochemical reactions with oxygen using exchange broadening in the ESR spectra of nitroxide radicals. Biochim Biophys Acta 460:152–156
13. Sarna T, Duleba A, Korytowski W, Swartz H (1980) Interaction of melanin with oxygen. Arch Biochem Biophys 200:140–148
14. Lai C-S, Hopwood LE, Hyde JS, Lukiewicz S (1982) ESR studies of O_2 uptake by Chinese hamster ovary cells during the cell cycle. Proc Natl Acad Sci USA 79:1166–1170
15. Halpern HJ, Peric M, Nguyen TD, Spencer DP, Teicher BA, Lin YJ (1990) Selective isotopic labeling of a nitroxide spin label to enhance sensitivity for T_2 oxymetry. J Magn Reson 90:40–51
16. Ardenkjær-Larsen JH, Laursen I, Leunbach I, Ehnholm G, Wistrand LG, Petersson JS, Golman K (1998) EPR and DNP properties of certain novel single electron contrast agents intended for oximetric imaging. J Magn Reson 133:1–12
17. Rogozhnikova OY, Vasiliev VG, Troitskaya TI, Trukhin DV, Mikhalina TV, Halpern HJ, Tormysheva VM (2013) Generation of trityl radicals by nucleophilic quenching of tris(2,3,5,6-tetrathiaaryl)methyl cations and practical and convenient large-scale synthesis of persistent tris(4-carboxy-2,3,5,6-tetrathiaaryl)methyl radical. Eur J Org Chem 2013:3347–3355
18. Dhimitruka I, Velayutham M, Bobko AA, Khramtsov VV, Villamena FA, Hadad CF, Zweier JL (2007) Large scale synthesis of a persistent trityl radical for use in biomedical

EPR applications and imaging. Bioorg Med Chem Lett 17:6801–6805

19. Halpern HJ (2003) Stable soluble paramagnetic compounds. in Berliner LJ (ed) In Vivo EPR (ESR): Theory and Applications, Kluwer Academic/Plenum Publishers, New York, pp 201–232
20. Ahn KH, Halpern HJ (2007) Spatially uniform sampling in 4-D EPR spectral-spatial imaging. J Magn Reson 185:152–158
21. Matsumoto K, Chandrika B, Lohman JAB, Mitchell JB, Krishna MC, Subramanian S (2003) Application of continuous-wave EPR spectral-spatial image reconstruction techniques for in vivo oxymetry: comparison of projection reconstruction and constant-time modalities. Magn Reson Med 50:865–874
22. Subramanian S, Devasahayam N, Murugesan R, Yamada K, Cook J, Taube A, Mitchell JB, Lohman JAB, Krishna MC (2002) Single-point (constant-time) imaging in radiofrequency Fourier transform electron paramagnetic resonance. Magn Reson Med 48:370–379
23. Epel B, Bowman MK, Mailer C, Halpern HJ (2014) Absolute oxygen R_{1e} imaging in vivo with pulse electron paramagnetic resonance. Magn Reson Med 72:362–368
24. Matsumoto S, Hyodo F, Subramanian S, Devasahayam N, Munasinghe J, Hyodo E, Gadisetti C, Cook JA, Mitchell JB, Krishna MC (2008) Low-field paramagnetic resonance imaging of tumor oxygenation and glycolytic activity in mice. J Clin Invest 118:1965–1973
25. Epel B, Sundramoorthy SV, Barth ED, Mailer C, Halpern HJ (2011) Comparison of 250 MHz electron spin echo and continuous wave oxygen EPR imaging methods for in vivo applications. Med Phys 38:2045–2052
26. Hyodo F, Matsumoto S, Devasahayam N, Dharmaraj C, Subramanian S, Mitchell JB, Krishna MC (2009) Pulsed EPR imaging of nitroxides in mice. J Magn Reson 197: 181–

185

27. Elas M, Williams BB, Parasca A, Malier C, Pelizzari CA, Lewis MA, River JN, Karczmar GS, Barth ED, Halpern HJ (2003) Quantitative tumor oxymetric images from 4D electron paramagnetic resonance imaging (EPRI): Methodology and comparison with blood oxygen level-dependent (BOLD) MRI. Magn Reson Med 49:682–691
28. Kuppusamy P, Chzhan M, Samouilov A, Wang P, Zweier JL (1995) Mapping the spin-density and lineshape distribution of free radicals using 4D spectral-spatial EPR imaging. J Magn Reson Ser B 107:116–125
29. Gorodetsky AA, Kirilyuk IA, Khramtsov VV, Komarov DA (2016) Functional electron paramagnetic resonance imaging of ischemic rat heart: Monitoring of tissue oxygenation and pH. Magn Reson Med 76:350–358
30. Redler G, Barth ED, Bauer KS, Jr., Kao JPY, Rosen GM, Halpern HJ (2014) In vivo electron paramagnetic resonance imaging of differential tumor targeting using cis-3,4-di(acetoxymethoxycarbonyl)-2,2,5,5-tetramethyl-1-pyrrolidinyloxyl. Magn Reson Med 71:1650–1656
31. Subramanian S, Devasahayam N, Matsumoto S, Saito K, Mitchell JB, Krishna MC (2012) Echo-based single-point imaging (ESPI): A novel pulsed EPR imaging modality for high spatial resolution and quantitative oximetry. J Magn Reson 218:105–114
32. Franken NAP, Rodermond HM, Stap J, Haveman J, van Bree C (2006) Clonogenic assay of cells *in vitro*. Nat Protoc 1:2315–2319
33. Suit HD, Suchato C (1967) Hyperbaric oxygen and radiotherapy of a fibrosarcoma and of a squamous-cell carcinoma of C_3H mice. Radiology 89:713–719
34. Sato-Akaba H, Fujii H, Hirata H (2008) Improvement of temporal resolution for three-dimensional continuous-wave electron paramagnetic resonance imaging. Rev Sci Instrum 79:123701

35. Sato-Akaba H, Kuwahara Y, Fujii H. Hirata H (2009) Half-life mapping of nitroxyl radicals with three-dimensional electron paramagnetic resonance imaging at an interval of 3.6 seconds. Anal Chem 81: 7501–7506

36. Kawada Y, Hirata H, Fujii H (2007) Use of multi-coil parallel-gap resonators for co-registration EPR/NMR imaging. J Magn Reson 184: 29–38

37. Jang H, Subramanian S, Devasahayam N, Saito K, Matsumoto S, Krishna MC, McMillan AB (2013) Single acquisition quantitative single-point electron paramagnetic resonance imaging. Magn Reson Med 70:1173–1181

38. Tofts PS (1997) Modeling tracer kinetics in dynamic Gd-DTPA MR imaging. J Magn Reson Imaging 7:91–101

39. Keana JFW, Hideg K, Birrell GB, Hankovszky OH, Ferguson G, Parvez M (1982) New mono- and difunctionalized 2,2,5,5-tetramethylpyrrolidine- and Δ^3-pyrroline-1-oxyl nitroxide spin labels. Can J Chem 60:1439–1447

40. Keana JFW, Pou S, Rosen GM (1987) Nitroxides as potential contrast enhancing agents for MRI application: influence of structure on the rate of reduction by rat hepatocytes, whole liver homogenate, subcellular fractions, and ascorbate. Magn Reson Med 5:525–536

41. Miyake M, Shen J, Liu S, Shi H, Liu W, Yuan Z, Pritchard A, Kao JPY, Liu KJ, Rosen GM (2006) Acetoxymethoxycarbonyl nitroxides as electron paramagnetic resonance proimaging agents to measure O_2 levels in mouse brain: a pharmacokinetic and pharmacodynamic study. J Pharmacol Exp Ther 318:1187–1193

42. Burks SR, Bakhshai J, Makowsky MA, Muralidharan S, Tsai P, Rosen GM, Kao JPY (2010) $^{2}H,^{15}N$-substituted nitroxides as sensitive probes for electron paramagnetic resonance imaging. J Org Chem 75:6463–6467

Figure captions

Fig. 1

(a) Chemical structures of 3,4-dicarboxy-2,2,5,5-tetra($^2H_3$)methylpyrrolidin-(3,4-$^2H_2$)-1-oxyl (^{2}H-DCP) and 3,4-dicarboxy-2,2,5,5-tetra($^2H_3$)methylpyrrolidin-(3,4-$^2H_2$)-(1-^{15}N)-1-oxyl (^{2}H,^{15}N-DCP). First-derivative EPR absorption spectra of ^{2}H-DCP (b) and ^{2}H,^{15}N-DCP (c) measured by 750-MHz EPR spectroscopy. Solutions (2 mM) of ^{2}H-DCP and ^{2}H,^{15}N-DCP were prepared in phosphate-buffered saline (PBS), and the pH was adjusted to 7.4.

Fig. 2

Survival fraction of murine squamous cell carcinoma (SCC VII) cells in the presence of ^{2}H-DCP (*n*=3). The closed plots and error bars show the means and standard deviations.

Fig. 3

In vivo time-course of the EPR signal intensities of intravenously injected ^{2}H,^{15}N-DCP and ^{2}H-DCP radicals (0.2 mmol/kg body weight for each probe) measured in the tumor-bearing hind leg of a mouse. The time-window of EPR image acquisition (7.5 min) is indicated in the time-course of the EPR signal intensity.

Fig. 4

In vivo EPR imaging of ^{2}H,^{15}N-DCP. (a) Photograph of the tumor-bearing hind leg of a subject mouse. (b) Surface-rendered image of the tumor-bearing hind leg of a subject mouse. (c) Slice-selective intensity maps. (d) Transverse relaxation time T_2^* maps corresponding to the intensity maps in Fig. 4(c). The field-of-view (FOV) of the 3D image is 58.3 mm, and the image matrix size is 64 × 64 × 64.

Figure 1

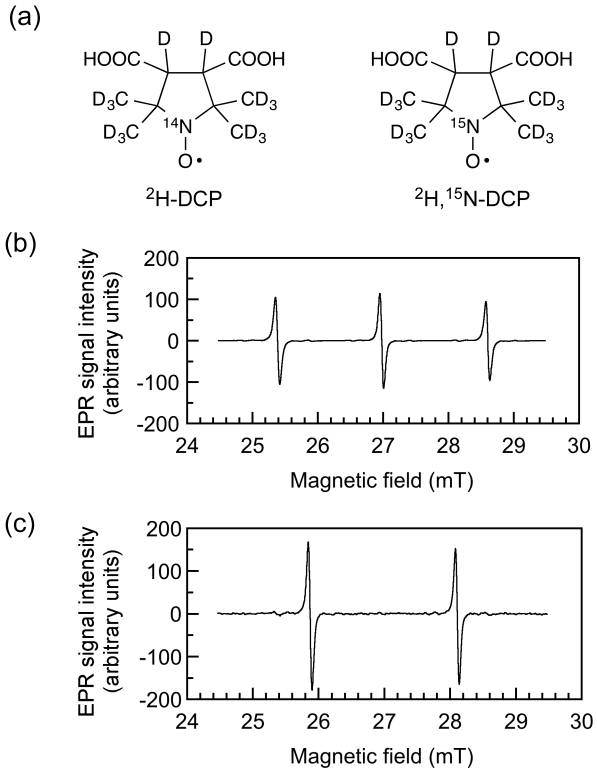

Figure 2

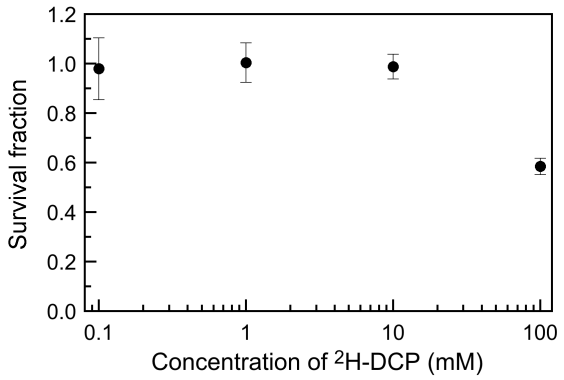

Figure 3

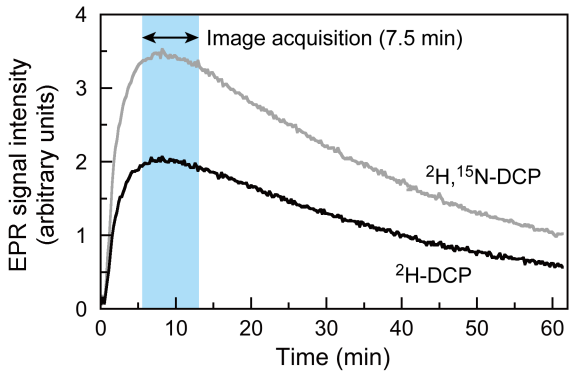

Figure 4